Dynamical characterization of one-dimensional stationary growth regimes in diffusion-limited electrodeposition processes

C. Léger, J. Elezgaray, and F. Argoul
Centre de Recherche Paul Pascal, Avenue Schweitzer, 33600 Pessac, France
(Received 29 May 1998)

The occurrence of stationary growth regimes in thin gap electrodeposition experiments is discussed in terms of diffusion-limited dynamics and confirmed by a quantitative interferometric analysis of concentration fields during copper electrodeposition in 50-μm cells, with unsupported electrolytes. We develop a 1D model for the time evolution of the averaged concentration profile after Sand's time and we check its predictions during the transitory and asymptotic growth regimes in electrodeposition experiments. [S1063-651X(98)15112-7]

PACS number(s): 81.15.Pq, 68.35.Rh, 61.43.Hv, 42.87.Bg

I. INTRODUCTION

The occurrence of diffusion-limited dynamics in growth experiments [1] such as electrodeposition was suggested by theoreticians in the early eighties. The publication of the diffusion-limited aggregation (DLA) model by Witten and Sander [2,3] initiated many experimental attempts to recover the type of morphologies that can be obtained with this model. Electrodeposition experiments proved to be particularly well suited for such studies, precisely because of their (apparent) simplicity and the richness and diversity of morphologies that could be obtained with them.

Beyond the characterization of the scale invariance properties of the morphologies of electrodeposition aggregates by sophisticated techniques [1,4–6], the analysis of the transport mechanisms and their influence on the morphology leaves many unanswered fundamental questions. Several attempts [7–12] have been made to develop a clear picture of electrodeposition in thin gap geometries. These studies focus on dense branching morphologies (DBM) that are characterized by a dense array of branches defining a flat front advancing at constant velocity through the cell, as illustrated in Fig. 1 with copper deposits. Three examples of DBM, obtained with three copper salts: (a) copper nitrate, (b) copper acetate, and (c) copper chloride are reported in Fig. 1. Although the DBM cannot be considered as homogeneous at small scales, its growth dynamics has been described by a one-dimensional (1D) process in the literature. Two types of models have been considered independently. The first of those [9,10] relies on the assumption that the electrochemical cell behaves as an Ohmic conductor, and that transport of electroactive species is driven solely by electric forces. The second model [12] is more general since it accounts for both diffusion and electric forces and it is built on the assumption of local electroneutrality on distances beyond the double layer. Despite their apparent differences, these two models lead their authors to identical conclusions, in particular, for the expression of the growth velocity with respect to the bulk electric field.

In this paper, we aim at demonstrating, based on experimental interferometric measurements of concentration maps, that these stationary growth regimes can be fully described in terms of diffusion-limited processes. In Sec. II, we review the previous approaches and propose a complete set of equations for modeling steady growth regimes in electrodeposition. In a third section, we present an experimental demonstration of the diffusive nature of these growth regimes by direct measurements of concentration profiles with a Mach-Zehnder interferometer. We show quantitatively the existence of quasi-one-dimensional stationary regimes in thin gap cells. We discuss the nature of the transitory regimes leading to stationary growth regimes and the limit of applicability of the 1D model to these intermediate phases.

II. MODELING APPROACHES

The complete set of equations that describe diffusion-limited electrodeposition can be found in theoretical articles that appeared in the early eighties [13], focusing on the nature of the initial instability of a flat surface by electrodeposition. We have also contributed recently by proposing a nonstationary analysis of this instability in galvanostatic (fixed current) regimes [14]. Here we focus on nonlinear growth regimes, which occur at long times, beyond the instability. The study of these regimes can be simplified when the system reaches a quasistationary growth, that is, a flat dense set of branches growing at constant velocity (the DBM).

The approaches of Fleury *et al.* [9] and Melrose [10] rely fundamentally on a purely Ohmic model, which does not account for the diffusion layer close to the cathode. According to these authors, at a given current density, the conductivity of the electrolyte imposes the electric field everywhere in the cell. The speed at which the anions leave the neighborhood of the cathode is $v_- \sim u_- E$ where u_- is the mobility of the anions and E the bulk electric field. The interfacial velocity is slaved to the speed of the anions to prevent the depletion of anions close to the cathode and the consequent formation of a space charge, introduced in this context by Chazalviel [7]: in order to avoid the formation of large electric fields, the cathode must grow at the withdrawal speed of the anions. The velocity of the interface is then $v_{deposit} \sim u_- E$. With this assumption, Fleury *et al.* [9] infer the dependence of the growth speed and the copper ratio of the deposit (its density) with respect to current density and bulk electrolyte concentration. These predictions have, moreover,

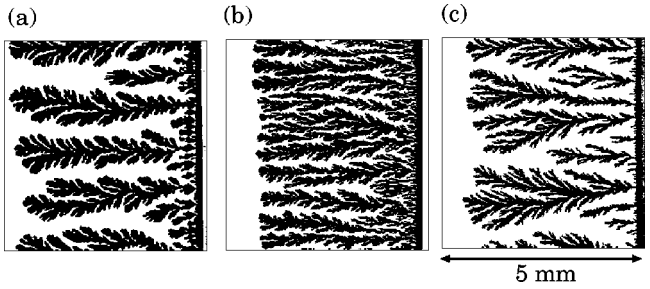

FIG. 1. Morphologies of copper deposits obtained with different anions. (a) $[Cu(NO_3)_2]=0.5$ mol l^{-1}, $j=50$ mA cm^{-2}, (b) $[Cu(CH_3COO)_2]=0.2$ mol l^{-1}, $j=12$ mA cm^{-2}, (c) $[CuCl_2]=0.5$ mol l^{-1}, $j=27$ mA cm^{-2}.

been confirmed by thorough experimental study of copper electrodeposition [8–11].

In a more recent paper Bazant [12] analyzes electrodeposition experiments in terms of a diffusive wave regulated process and proposes a 1D stationary solution for diffusion-limited electrodeposition that was, incidentally, suggested by Barkey in [15]. Our approach is closer to Bazant's since we aim at demonstrating that there is no need for neglecting diffusion processes to recover the simple relation that links the velocity of the cathode with the bulk electric field. In this section, we derive in a simpler way the equations obtained by Bazant [12].

The modeling of single salt electrodeposition processes in thin gap cells (where buoyancy-driven convection can be neglected [16–19]) is founded on the assumption that electroneutrality prevails beyond the double layer, and that a single diffusion equation can be recovered [20] in the laboratory frame:

$$\partial_t C = D\nabla^2 C. \tag{1}$$

In this equation an ambipolar diffusion coefficient $D=\{z_+u_+D_- - z_-u_-D_+\}/\{z_+u_+ - z_-u_-\}$ accounts for both diffusion and migration since when electroneutrality is fulfilled the migration term in $\partial_t C$ becomes proportional to the diffusion term (Laplacian of the concentration), $C=z_+C_+ = |z_-|C_-$ is the equivalent concentration, D_+ and D_- are the diffusion coefficients corresponding, respectively, to the cations and anions, whereas u_+ and u_- stand for their mobility, $u_\pm = D_\pm/RT$ [20] and z_+ and z_- (algebraic quantities) their respective charges.

The expressions of the flux density in the bulk of the electrochemical cell (far from the electrodes) read

$$|z_\pm|\vec{J}_\pm = -D_\pm\vec{\nabla}C - z_\pm D_\pm C\vec{\nabla}\Phi, \tag{2}$$

where $\Phi = F\phi/RT$ is the nondimensional electric potential (F is the Faraday constant) and the advection term is neglected.

The boundary conditions for fluxes and growth velocity are given by conservation laws and experimental constraints. In the case of galvanostatic experiments, the flux density of cations $\vec{J}_+$ is fixed to be proportional to the current density on the interface. If z_+ is the number of electrons exchanged in the reduction reaction and $\vec{j}$ the current density,

$$\vec{J}_{+el} = \vec{j}/(z_+F) = -\frac{D}{1-t^+}\vec{\nabla}C_+\bigg|_{el} - \frac{C_+|_{el}\vec{v}_{el}}{1-t^+}, \tag{3}$$

where $\vec{v}_{el}$ is the speed of the electrode relative to the surrounding fluid and t^+ the transference number of the cations $t^+ = z_+D_+/(z_+D_+ - z_-D_-) = z_+u_+/(z_+u_+ - z_-u_-)$. This equation is straightforwardly obtained through the assumption that the interfacial flux of anions is zero [20]. The second boundary equation describes the local conservation of copper species during the electrodeposition:

$$-\rho_{copper}\vec{v}\cdot\vec{n} = M\vec{J}_{+el}\cdot\vec{n}, \tag{4}$$

where M is the molar mass of copper, ρ_{copper} the copper density of the deposit, and $\vec{n}$ the normal to the deposit interface.

In this section, we assume that the system rapidly converges towards a stationary growth regime and we analyze the properties of the growth in such a case. Before deriving the analytical expression for the steady concentration profile, we would like to point out several important issues. In the following, we assume the existence of a 1D solution to Eqs. (1)–(4), and compare it with the steady-state regime observed in experiments. The 1D model is, by assumption, invariant along the direction of the electrode, whereas the experimental system is invariant only on the average or, more precisely, when averaged over scales that are larger than the typical distance between fingers. The fact that, upon averaging, the evolution equations look the same as Eqs. (1)–(4) is by no means obvious and should be considered as a first assumption. This (implicit) coarse graining of the equations has several consequences: (i) the density ρ_{copper} in Eq. (4) has to be replaced by some effective density $\overline{\rho}$. (ii) We have shown in [14] that a flat advancing (2D) front is unstable for the set of equations (1)–(4). However, we show below that the 1D front solution of these equations matches quite well the experimentally observed advancing front, which is clearly stable. This paradox can be understood if one assumes that the coarse graining procedure introduces additional stabilizing terms, probably dependent on the local curvature, that modify the linear stability analysis. Again this issue is completely overlooked in the present paper, although we think that its understanding will be a key issue in further developments.

In a general way, given the velocity v of the 1D growth (whether constant or not), one can write a coordinate change $\zeta(t) = x - x(t)_{front} = x - \int_0^t v(u)du$, where x is the direction of the growth (one dimensional) and $v(t)$ its velocity. Under this coordinate change, the diffusion equation (1) comprises an additional term describing the translation of the frame:

$$\partial_t\tilde{C} = D\partial^2_{\zeta^2}\tilde{C} + v(t)\partial_\zeta\tilde{C}. \tag{5}$$

We have adopted the ~ notation for the moving frame. Given the experimental evidence for constant growth speed regimes reported in the literature [9,10], it seems reasonable to look for a stationary solution of this partial differential equation in the moving frame:

$$\partial_t\tilde{C} = 0 = D\partial^2_{\zeta^2}\tilde{C} + v\,\partial_\zeta\tilde{C}. \tag{6}$$

In this model, we make the hypothesis that the number of exchanged electrons during the reduction process is equal to the charge of the cation to avoid discussing the reduction of other species such as protons [21–24], which is far beyond the scope of this article. The boundary condition (3) reads

$$z_+\tilde{J}_+|_{\zeta=0}=\frac{j}{F}=-\frac{\tilde{C}|_{\zeta=0}v}{1-t^+}-D\frac{\partial_\zeta\tilde{C}|_{\zeta=0}}{1-t^+}, \tag{7}$$

where $\tilde{J}_+$, replacing $\vec{J}_+$ denotes the one-dimensional flux density in the moving frame. Equation (6) can be straightforwardly solved, given the boundary concentrations $\tilde{C}(\zeta\to\infty)=C_\infty=z_+C_{+\infty}$ ($C_{+\infty}$ is the initial bulk concentration prior to growth) and $\tilde{C}_{\zeta=0}=C_0$ an arbitrary value. We have shown previously [14] that in galvanostatic deposition experiments, the fastest instability of the interface arises for small but non-null values of C_0 (prior to Sand's time, defined as the time when the interfacial concentration is equal to zero [25]). The solution of Eq. (6) for the concentration in the moving frame reads

$$\tilde{C}(\zeta)=C_\infty+(C_0-C_\infty)e^{-(\zeta/l_d)},\quad l_d=\frac{D}{v}. \tag{8}$$

Such an equation has previously been derived by Barkey [15] in a short note in 1990, and more recently by M. Bazant [12] with arguments similar to those developed here. Replacing the expressions for $\partial_\zeta\tilde{C}|_{\zeta=0}=(C_\infty-C_0)/l_d$ in Eq. (7), we recover the relation between the growth velocity and the current density j:

$$v=-(1-t^+)\frac{j}{FC_\infty}. \tag{9}$$

The mean density $\overline{\rho}$ of the aggregate, averaged over the direction of the electrode, is easily derived from Eqs. (4) and (9): $\overline{\rho}=MC_\infty/z_+(1-t^+)$, as previously found in Ref. [9]. To relate the growth speed to the bulk electric field, we must analyze the flux equations far from the deposit, where the concentration gradient becomes negligible. In the moving frame the flux equations read

$$|z_\pm|\tilde{J}_\pm=-\tilde{C}v-D_\pm\partial_\zeta\tilde{C}-z_\pm D_\pm\tilde{C}\partial_\zeta\tilde{\Phi}. \tag{10}$$

The total current density is the sum of the partial current densities for each ion:

$$\begin{aligned} j/F&=z_+\tilde{J}_++z_-\tilde{J}_-\\ &=-(D_+-D_-)\partial_\zeta\tilde{C}-(z_+D_+-z_-D_-)\tilde{C}\partial_\zeta\tilde{\Phi}. \end{aligned} \tag{11}$$

Far from the cathode and the anode, $\partial_\zeta\tilde{C}$ is negligible and this equation models a purely Ohmic transport:

$$j/F=-(z_+D_+-z_-D_-)C_\infty\partial_\zeta\tilde{\Phi}|_{\zeta\to\infty}. \tag{12}$$

The velocity is therefore

$$\begin{aligned} v&=-(1-t^+)(z_+D_+-z_-D_-)\partial_\zeta\tilde{\Phi}|_{\zeta\to\infty}\\ &=-z_-D_-\partial_\zeta\tilde{\Phi}|_{\zeta\to\infty}=z_-Fu_-\tilde{E}_\infty, \end{aligned} \tag{13}$$

with $\tilde{E}_\infty=-\partial_\zeta\tilde{\phi}|_\infty=-RT\partial_\zeta\tilde{\Phi}|_\infty/F$. This equation is similar to those of Fleury *et al.* [9], Melrose [10], and Bazant [12] and has been obtained under the assumption that the number of exchanged electrons in the reduction process is equal to the charge of the cation. The difference between our approach and the two first quoted references comes from the fact that we derive the equation for the growth velocity directly from the 1D equations and that, moreover, we show that the predictions of the 1D model for the concentration profile can be quantitatively checked against the experiment. Equation (13) is nevertheless misleading because it gives the reader the feeling that the only relevant parameter is the mobility of the anions. To derive the interfacial velocity, we used only the value of the interfacial concentration gradient, which depends on the current and on the mobilities of anions and cations [$D=f(u_+,u_-)$; $t^+=f(u_+,u_-)$]. Part of these parameters are hidden when the velocity is expressed as a function of the bulk electric field instead of the current density, indeed, the bulk electric field is not an independent parameter contrary to the current density.

To conclude this section, in view of Sec. III D devoted to buoyancy driven convection systems, it is worth remarking that Eq. (13) can be directly deduced from Eqs. (10) and (12), with the assumption that the 1D flux of cations is, under the steady growth regime, independent of the space variable ζ, which amounts to equating the flux of cations far from the growth (beyond the diffusion layer) with the flux of cations on the interface: $\tilde{J}_+=j/(z_+F)$.

III. EXPERIMENTAL RESULTS

A. Experimental setup

The experiments are performed in cells made of two closely spaced optical flat glass plates ($\lambda/4$ over $50\times50\ \mathrm{mm}^2$), whose interspace is filled with a single metal electrolyte, without a supporting electrolyte. Two straight parallel ultrapure copper, platinum, or silver wires (50 μm diameter, Goodfellow 99.0% purity) are tightly confined between the two glass plates and play the role of both spacers and electrodes. The solutions of copper nitrate, chloride, and acetate (ACS reagent) are prepared from deionized water, carefully cleaned of any trace of dissolved oxygen by bubbling nitrogen through it for 1 h. All of the experiments are performed at fixed current intensity and at room temperature ($\sim$20 °C). In all experiments, the anode is made of a pure copper wire. With copper nitrate, the cathode is made of silver and 1% $CuCl_2$ is added to the $Cu(NO_3)_2$ electrolyte to avoid the passivation of the cathode with copper hydroxide prior to the onset of the growth. With copper chloride, a Pt cathode improves its resistance to corrosion. With copper acetate, the anodic compartment of the cell is filled by a dilute solution to avoid a precipitation of the salt due to saturation effects by dissolution of the anode and the cathode is made of silver.

A phase shift Mach-Zehnder interferometer is independently used to resolve the concentration field, averaged on the depth of the cell. A sketch of the phase shift Mach-Zehnder interferometer can be found in Ref. [16]. The interference patterns are recorded through a charge-coupled device (CCD) camera coupled to a frame grabber [26] with a

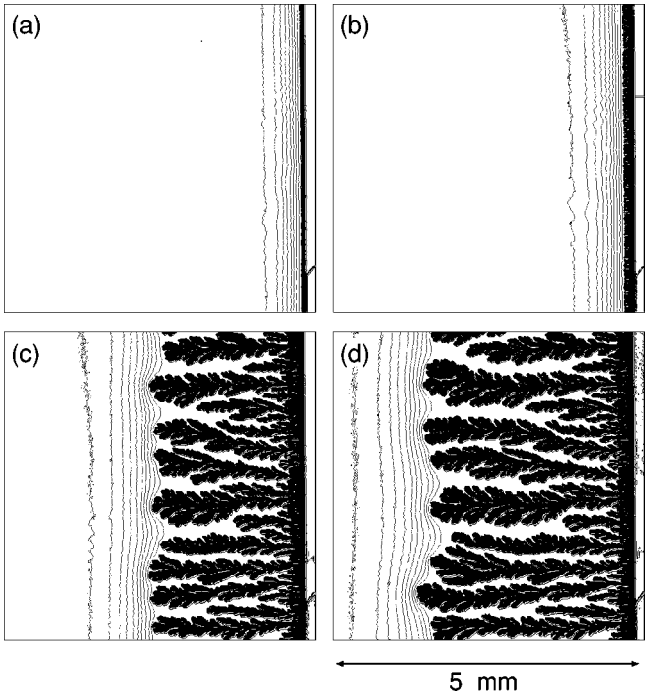

FIG. 2. Four successive pictures of the electrodeposition clusters superimposed to the isoconcentration contours obtained by the phase-shift interferometry technique (a) $t/t_S=0.7$, (b) $t/t_S=1.3$, (c) $t/t_S=8.9$, (d) $t/t_S=10$. $[Cu(NO_3)_2]=0.5$ mol l^{-1}, $j=48$ mA cm^{-2}.

768×512 pixel resolution. The great advantage of phase shift versus standard interferometry comes from the fact that it provides an accurate reconstruction of the whole concentration map from a set of successive interference pictures recorded for shifted values of the phase difference between the two wave fronts of the interferometer, and that it can also be used as an holographic interferometer [27]. Figure 2 illustrates the isoconcentration curves reconstructed from the interferometric measurements at four successive times of the electrodeposition of copper in a 50-μm gap cell. The difference between these isoconcentration curves has been chosen equal to $C_\infty/10$ mol l^{-1} for clarity of this illustration. The confinement of the cell ensures the damping of the buoyancy driven convection [16,17,19]. The sizes of the cell are $W=5$ cm, $L=5$ cm, $\delta=50$ μm. The length of the cell is much greater than the zone inspected by interferometry (5 mm) to get rid of any perturbation of the growth by anodic processes.

B. Description of stationary growth regimes in electrodeposition: experimental results

DBM are the result of at least four successive stages that bring a flat electrode into a dense forest of branched trees, such as shown in Fig. 1. These stages can be easily identified from the temporal evolution of the cell potential, such as shown in Fig. 3.

After the current is switched on, the cathodic interfacial concentration begins to decrease. During this early stage, the cathodic concentration profile can be quantitatively understood as the solution of the diffusion equation with constant interfacial flux [16]. The cell voltage results from both Ohmic drop and interfacial kinetic polarization contributions.

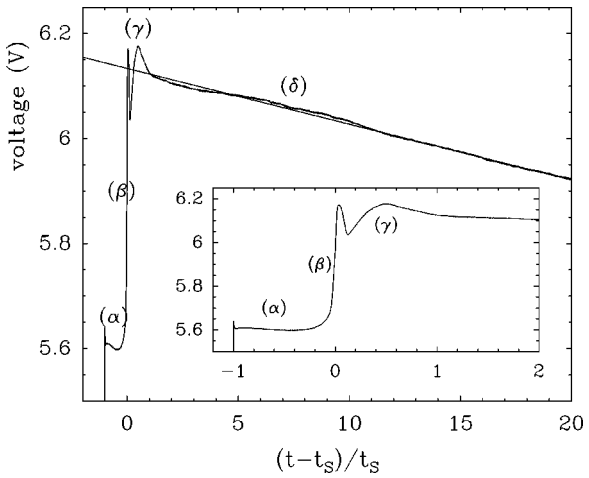

FIG. 3. Temporal evolution of the voltage of the cell. $[Cu(NO_3)_2]=0.5$ mol l^{-1}, $j=65$ mA cm^{-2}. The time has been rescaled by Sand's time $t_S\sim33$ s.

They do not change much during this first stage so that the cell potential exhibits a plateau at the beginning of the experiment (Fig. 3, phase α).

When the interfacial concentration approaches zero, the potential progressively increases (phase β in Fig. 3). This divergence is not really surprising and can be explained by two types of arguments: (i) the Ohmic resistance of the cathodic diffusion layer increases when the concentration decreases [28]; (ii) the Butler-Volmer equation predicts an increase of cathodic overpotential when the interfacial concentration decreases. Very close to Sand's time, the interface becomes highly unstable [14] and develops into a forest of fine spikes. The cell voltage suddenly decreases due to the sharp acceleration of the growth velocity (phase γ of Fig. 3). Since the global mass deposition rate remains constant during the experiment, the increase of the interfacial velocity enhances the porosity of the deposit. The voltage evolves in a complex way during this selection regime; its shape depends on the anion.

We focus in this section on the subsequent stationary regime, characterized by a constant interfacial velocity, leading to a linear relation between time and cell voltage (phase δ of Fig. 3). From the slope of the voltage curve during this steady regime, one can get an estimation of the deposit velocity, as already discussed in Ref. [9]. For instance, in the experiment of Fig. 3, this velocity has been estimated to 5 μm/s, in agreement with its direct measurement from the digitized pictures of the growth (~4.6 μm/s) [9]. In Fig. 2 we show four successive snapshots of the copper deposit superimposed on the concentration isocontours computed from interferometric measurements. These pictures illustrate the successive events discussed above: the interfacial depletion [Fig. 2(a)], the destabilization [Fig. 2(b)], and the subsequent invasion of the cell by the copper fingers [Figs. 2(c) and 2(d)]. We observe that the isoconcentration lines are roughly parallel to the electrode up to a few tens of microns of the tips of the ''trees.'' We also remark that the back sides of the ''trees'' are completely depleted in copper salt. With this enlargement, two different scales can be distinguished. The smallest scale, which corresponds to the width of the spikes [Fig. 2(b)] which emerge from the electrode, can be

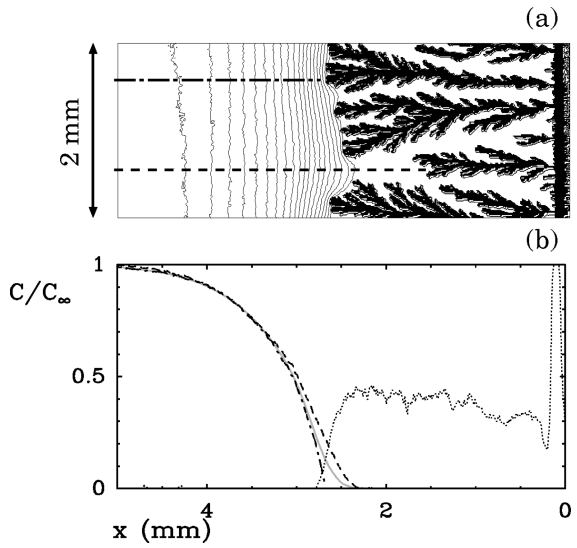

FIG. 4. Illustration of the concentration profile extraction by interferometry. (a) Snapshot of the 2D isoconcentration contours with the deposit picture on which the location of the two section planes has been added. (b) Concentration fronts corresponding respectively to section planes of (a) in dashed and dashed-dotted lines, and to the average (in gray) of the concentration profiles along the direction of the electrode. In dotted lines, the occupation ratio of the deposit in the cell is also represented. The parameter values are identical to Fig. 1(c).

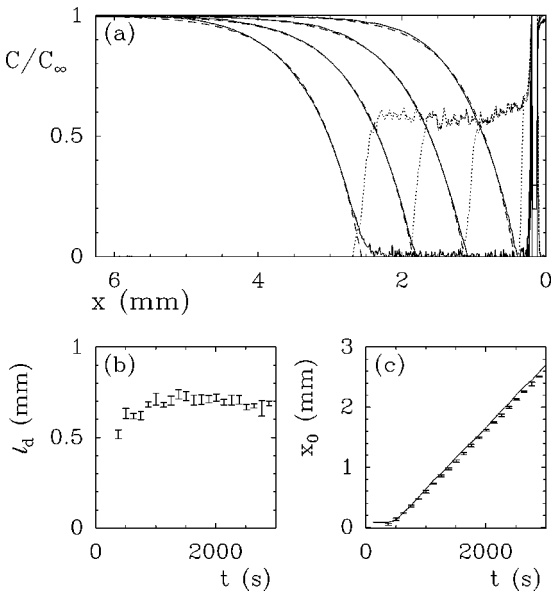

FIG. 5. Stationary growth regime in the electrodeposition of copper acetate. (a) Concentration profiles extracted from experimental data (plain curve) fitted by the exponential stationary profile [Eq. (8)] (dashed curves), time interval between successive profiles: 630 s. The ratio of sites occupied by the aggregate is plotted with a dotted line. (b) Temporal evolution of the fitted diffusion length. (c) Temporal evolution of the deposit length computed from the deposit picture (plain curve) or from the fit of the experimental concentration profiles with Eq. (8) (symbols). The parameter values are identical to Fig. 1(b).

considered as a capillary length. It is much smaller (about ten times) than the average width of the final trees. The dense branching morphology term can be invoked in this case because the distance separating two neighboring trees is much smaller than their height in Fig. 2(d).

In all the experiments discussed hereafter, the length of the diffusion layer (depletion zone) is much greater than the thickness of the cell. Since, moreover, the transport is diffusive, we assume that the concentration gradients in a direction perpendicular to the glass plates can be neglected. The concentration field can reasonably be considered as 2D and our 2D interferometric measurements are therefore particularly adapted. Moreover, in the case of dense patterns, the distance between the branches of the deposit is smaller than the size of the depleted zone. Far from the deposit, the concentration depends essentially on the distance to the deposit, so that the concentration field can be considered to be one dimensional. These experimental observations justify qualitatively the 1D modeling. In the forthcoming, we present quantitative evidence for the existence of stationary quasi-1D growth regimes during copper electrodeposition in thin gap cells.

In Fig. 4, we describe the method of extraction of concentration profiles and their averaging along the width of the cell. On the top panel of Fig. 4(a) the locations of two sections are marked by dashed lines and the corresponding concentration profiles are plotted with the same dashing on Fig. 4(b). In gray, between these two profiles, the averaged concentration profile computed by summing the concentration along a parallel axis to the electrode and normalizing it by the width of the free zones (coded in white). The aggregate occupation ratio, computed as the ratio of the sum of black pixels with respect to the total number of pixels for each abscissa x (the width of the electrode on the digitized picture), is reported with a dotted line. The plateau in the aggregate occupation ratio profile beyond 1 mm indicates that the growth has reached a stationary regime. The front part of this occupation ratio profile (front of the deposit) shows a decay that depends on the fluctuations in the sizes of the trees. In Figs. 5 and 6 we present a quantitative analysis of the stationary growth regime for copper acetate and copper nitrate. On the top panels are reproduced the averaged concentration profiles (plain lines) fitted by the equation $C_\infty+(C_0-C_\infty)(1-e^{-[(x-x_0)/l_d]})$ in dashed lines, the experimental profile parametrization is performed by adjusting both the diffusion length l_d and the growth interface position x_0 at each time. The aggregate occupation ratio profiles are superimposed in dotted lines. The fitted diffusion lengths l_d are plotted versus time in Figs. 5(b) and 6(b). In (c) of Fig. 5 and of Fig. 6 the temporal evolution of the interface front position x_0 is reported. These two figures demonstrate unambiguously that the system reaches a stationary growth regime, characterized by a constant speed and a steady concentration profile. Moreover, this phenomenon is robust since we show that it is reproduced independently of the copper salt. The generic character of these stationary dynamics is shown in Fig. 7 where we have gathered the experiments with copper nitrate (black triangle) and copper acetate (gray squares). It illustrates the equality (up to experimental uncertainties) of the fitted diffusion length l_d and the ratio D/v, computed from the measured deposit velocity in the asymptotic regime, with the ambipolar diffusion coefficient equal to 10^{-5} cm^2 s^{-1} for copper nitrate and 0.6 10^{-5} cm^2 s^{-1} for copper acetate, as measured independently

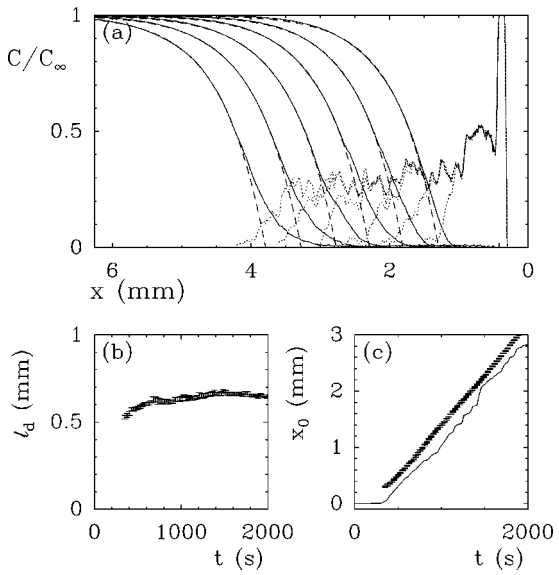

FIG. 6. Stationary growth regime in the electrodeposition of copper nitrate. (a) Concentration profiles extracted from experimental data (plain curve) fitted by exponential stationary profile [Eq. (8)] (dashed curves), time interval between successive profiles: 125 s. The ratio of sites occupied by the aggregate is plotted with a dotted line. (b) Temporal evolution of the diffusion length. (c) Temporal evolution of the deposit length, computed from the deposit picture (plain curve) or from the fit of the experimental concentration profiles with Eq. (8) (symbols). $[Cu(NO_3)_2]=0.75$ mol l^{-1}, $j=40$ mA cm^{-2}.

by our interferometry technique [16,29]. The error bars account for uncertainties on the values of the diffusion coefficient, the measured interfacial velocity, and the fitted diffusion length [Figs. 5(b) and 6(b)]. We note that the diffusion lengths are all greater than 100 μm, that is, greater than the depth of the cell (50 μm), which justifies afterwards that these processes can be considered as quasi-one-dimensional. In this figure the set of experiments corresponds to a range of current density: 10–80 mA cm^{-2} and of copper salt concentration $0.2M$ to $0.75M$. The smaller diffusion lengths have been obtained for greater current densities and smaller concentration of salt.

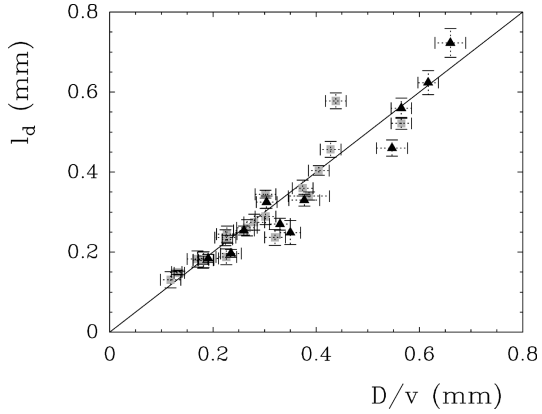

FIG. 7. Comparison of the fitted diffusion length from experimental concentration profiles with Eq. (8) and the measured velocity of the growth.

C. From the initial instability to the stationary regime: the transitory period

In the previous section, we determined the steady interfacial velocity by solving a one-dimensional transport equation in the frame moving at the speed of the deposit. In this section, we extend the relevance of the 1D model to the transitory regime that occurs just after the destabilization of the interface, prior to the stationary growth regime.

Before Sand's time t_S [25], a flat and compact interface advances in the laboratory frame with a velocity $v_{t<t_S}=-jM/z_+F\rho_{copper}$ (ρ_{copper} is the density of the compact copper deposit). In this growth regime, the interface displacement is transmitted to the fluid without modification; they both move at the same speed. In the moving frame, a simple diffusion equation is recovered for $t<t_S$.

After the destabilization, there is a sudden acceleration of the growth and a porous deposit advances in an almost motionless fluid with a velocity: $v(t)=-jM/z_+F\overline{\rho}(t)$. The transport equation in the moving frame includes the relative motion of the fluid with respect to the deposit and is similar to Eq. (5).

Looking for a stationary solution of Eq. (5), we found in Sec. II the asymptotic velocity $v(\infty)=-j(1-t^+)/FC_\infty=z_-Fu_-E_\infty$. The transition from the slow growth regime at $v_{t<t_S}$ to the stationary growth $v(\infty)$ is a fundamental issue that we discuss in the sequel, under the assumption of a 1D model. To simplify our discussion we make the following approximations: (i) v is negligible before Sand's time and will therefore be approximated to zero, since the deposit is very compact [14]. (ii) The interfacial concentration will be assumed to vary very slowly beyond Sand's time, in such a way that it can be considered as stationary. This follows from the fact that the interfacial concentration gets close to zero at Sand's time, and does not seem to change at longer times, as shown in Figs. 5 and 6.

In order to get an approximation of $v(t)$ after Sand's time, we have to solve Eq. (5) with the boundary conditions

$$\tilde{C}(\zeta=\infty,t)=C_\infty,$$

$$\tilde{C}(\zeta=0)=0,$$

$$\partial_\zeta\tilde{C}(\zeta,t)|_{\zeta=0}=-\frac{j(1-t^+)}{FD}, \tag{14}$$

and the initial condition

$$\tilde{C}(\zeta,t_S)=C_\infty+\frac{j(1-t^+)}{FD}\times\left\{2\sqrt{\frac{Dt}{\pi}}\exp\left(-\frac{\zeta^2}{4Dt}\right)-\zeta\ \mathrm{erfc}\left(\frac{\zeta}{2\sqrt{Dt}}\right)\right\} \tag{15}$$

with $\sqrt{t_S}=-FC_\infty\sqrt{\pi D}/[2j(1-t^+)]$. Equation (15) is the analytical solution of Eq. (1) for a fixed current reduction process, starting from an homogeneous concentration and written for $t=t_S$ [25]. The interfacial velocity just after Sand's time can be deduced by a straightforward computa-

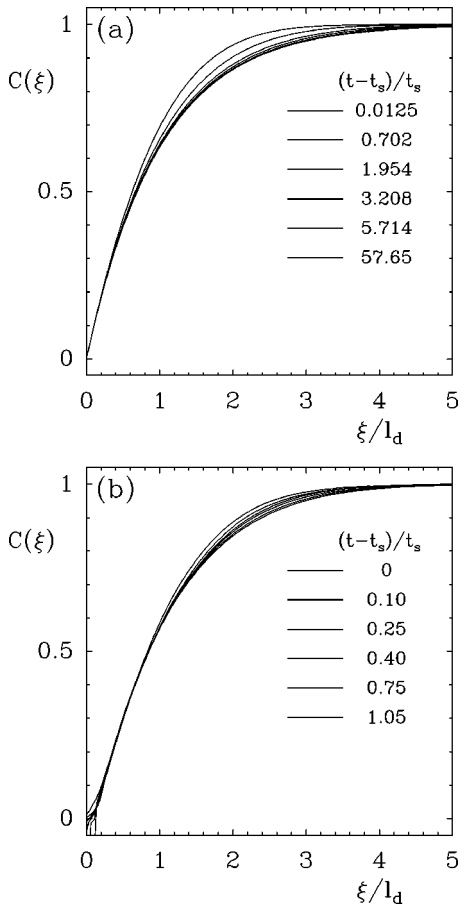

FIG. 8. Plot of the temporal evolution of the concentration profile in the transitory regime, from Sand's time to the stationary growth regime. (a) Numerical resolution of the 1D diffusion equation (5). (b) Experimental data obtained from electrodeposition of copper nitrate with the same parameters as in Fig. 6.

tion, assuming that $\partial_t \tilde{C}(\zeta=0,t)=0$. In that case the growth speed is related to the spatial derivatives of $\tilde{C}$ through

$$v(t=t_S)=\frac{-D\partial^2_{\zeta^2}\tilde{C}(\zeta,t_S)|_{\zeta=0}}{\partial_\zeta \tilde{C}(\zeta,t_S)|_{\zeta=0}} \tag{16}$$

with $\partial_\zeta \tilde{C}(\zeta,t_S)|_{\zeta=0}=-j(1-t^+)/FD$ and $\partial^2_{\zeta^2}\tilde{C}(\zeta,t_S)|_{\zeta=0}=j(1-t^+)/(FD\sqrt{\pi D t_S})$. One gets the relation

$$v(t=t_S)=-\frac{2j(1-t_+)}{F\pi C_\infty}=\frac{2v(t=\infty)}{\pi}. \tag{17}$$

This means that at Sand's time the interface velocity evolves instantaneously from a null value to a finite value when the interfacial concentration drops to zero. This unphysical discontinuity can be avoided if one assumes that the electrode gets unstable just before Sand's time [14]. Nevertheless, as observed in experiments, Sand's time corresponds to a sharp acceleration of the growth speed that is expressed in a very schematic form here, as a discontinuity. With a direct numerical simulation (finite difference scheme) of the diffusion equation (5), starting from the analytical solution (15) with $\tilde{C}(0)=0$, the temporal evolution of the concentration profiles can be computed numerically. We observe in Fig. 8(a) that the system spontaneously converges towards a stationary regime of growth where the concentration profile no longer changes. The temporal evolution of the growth speed, obtained by numerical simulations, is also given in Fig. 9. Figure 8(a) shows the similarity between the temporal evolution of the numerical concentration profiles and those extracted from the electrodeposition experiment [see Fig. 8(b)]. This shows that even in the transitory regime, the 1D model can be used as a first basis for predicting the characteristic relaxation time. A more precise verification of the similarity of the temporal behavior of both numerical profiles and experimental profiles is given in Fig. 10 where we have plotted the mean distance between each profile and the asymptotic profile with respect to time:

$$\sqrt{\int_0^\infty [C(\zeta,t)-C(\zeta,\infty)]^2 d\zeta}\Big/\sqrt{\int_0^\infty [C(\zeta,t_S)-C(\zeta,\infty)]^2 d\zeta}.$$

For the experimental plot (plain curve), we have computed the mean distance between each experimental profile at a given time with the best fit of the exponential solution. The essential conclusion of this figure is that in both theoretical (1D) and experimental cases, the characteristic duration of the transitory regime is close to the value of the Sand's time t_S. We also note in the insert of Fig. 10 that the distance to the asymptotic profile decays exponentially only for $t-t_S > 5t_S$, which means that one cannot capture the short time characteristics of the transitory period through the linear stability analysis of the asympotics. At that time, the correspondence between the 1D model and the experiment means that beyond Sand's time the diffusion layer has spread on length scales that are greater than the microscopic details of the deposit and that its global dynamics can be approximated by a 1D model.

D. From diffusion-limited to buoyancy driven convection-limited regimes

As shown in the previous section, the hypothesis of concentration field stationarity is suitable for understanding the velocity of the interface in the case of thin cells, in which buoyancy driven convection is negligible. However, the relation $v \sim u_- E$ has been checked for a large range of experimental parameters, including thick cells [9]. In this section, we show that during electrodeposition in thick cells, where the growth instability is driven by buoyancy driven convective diffusion, both concentration and velocity fields reach a steady state in the moving frame.

Using thick cells (>70 μm), the concentration gradients produced by reduction and oxidation on the cathode and anode, respectively, imply density gradients that induce, from each electrode, the propagation of convective rolls through the cell with a square root of time law [17,19]. As a consequence, the concentration of copper salt is no longer homogeneous along the direction perpendicular to the glass plates and the interferometric measurement can only capture its average along this direction. The shape of the concentration profiles computed by Chazalviel [19] is in good agreement

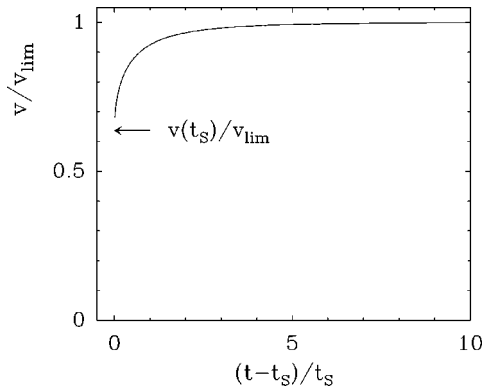

FIG. 9. Plot of the temporal evolution of the growth speed in the transitory regime, from Sand's time to the stationary growth regime computed by the numerical resolution of the 1D diffusion equation (5) with boundary conditions (17).

with optical measurements [19,30] during the period prior to electrode destabilization, but there has been no quantitative investigation of further growth regimes. Chazalviel proposed that at longer times, the deposit would grow at constant speed and would push away the depleted zone whose size would remain constant. This picture is in agreement with our concentration measurements in both thin (see Figs. 5 and 6) and thick (see below) cells. Figures 11 and 12 report the interferometric analysis of copper electrodeposition from copper sulfate $0.2M$ in a 250-μm cell. In Fig. 11, we plot the size of the deposit (mean front position) and of the depleted zone as a function of time. The size of the depleted zone is defined as the distance between the initial cathode position and the position in the cell where the concentration reaches 95% C_{bulk}. During the depletion period, we find that the size of the depleted zone scales as $t^{0.6}$ in close agreement with our preceding measurements [30] and Chazalviel's predictions [19]. After this induction period, both the deposit size and the length of the depleted zone increase linearly with

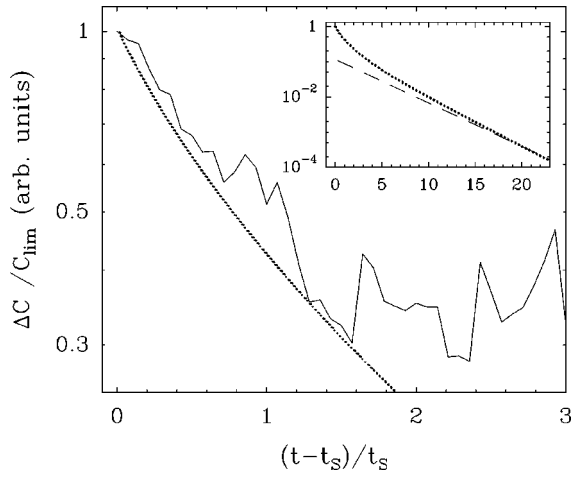

FIG. 10. Mean-square dispersion of concentration profiles with respect to the asymptotic profile (see text). In dotted line, the numerical resolution of the 1D diffusion equation (5), in plain line, the experimental data obtained from electrodeposition of copper nitrate, with the same parameters as in Fig. 6. In the inset, we show the numerical data for a longer time (dotted line) and the theoretical decay corresponding to a linear regime (dashed line).

time. Once again, the plots of Fig. 11 bring evidence for the occurrence of steady growth regimes in thick cells. To confirm this evidence, we plot in Fig. 12(a) the evolution of the 1D average concentration profiles in the laboratory frame. The convergence of these concentration profiles towards an asymptotic shape is illustrated in Fig. 12(b) where a shift of the abscisse at each time (adjustment by hand) allows the superimposition of all the concentration profiles.

With the same assumption as was done at the end of Sec. II (i.e., in the stationary regime the flux of cations is invariant in space) and from the fact that far enough from the electrode neighborhood, the buoyancy driven convection is negligible, we get the same linear relation (13) for v versus the bulk electric field.

E. Discussion of the occurrence of 1D dynamics

We performed experiments with sulfate, chloride, nitrate, and acetate copper salts. Compared to previous studies, we used concentrated solutions (from $0.2M$ to $0.75M$), in order to reach a good signal to noise ratio in the interferometric analysis. The minimal current used was close to 10 mA cm^{-2}. For smaller values, the growth is too slow to be performed in open cells. This current density corresponds to a growth speed of around one μm s^{-1}. The maximal current is limited by the requirement on the diffusion length to be larger than the thickness of the cell, $l_d = C_\infty FD/[|j|(1-t^+)] \gg \delta$, that is, $|j| \ll 400$ mA cm^{-2}. We therefore select the experiments with $|j|$ less than 100 mA cm^{-2}.

With copper acetate, nitrate and chloride, whatever the parameter range tested, we obtained deposits whose structural wavelength (mean distance between the trees) is of the order of or smaller than the diffusion length [Figs. 13(b), 13(c), and 13(d)], and where the aggregate envelope is easily defined, which validates the 1D analysis (as discussed in Figs 4–6). The situation is quite different in the case of copper deposition from copper sulfate salt, as illustrated in Fig. 13(a). In all the experiments performed with copper sulfate, the distance between the trees has been found to be larger than the diffusion length. In the deposit shown in Fig. 13(a), it is, moreover, larger than the size of the picture.

One important question remains, which concerns the actual convergence of the real experiment towards such stationary growth regimes. The fact that the numerical simulations show that in one dimension the system converges spontaneously towards a stationary regime shows simply that if in the experiment the trees that emerge from the instability of the interface do not perturb too much the diffusion layer in such a way that the system can still be approximated as a one-dimensional one, then the experiment is likely to converge towards a stationary regime. The physical reasons for this 1D behavior remain an open question. A complete simulation of a two-dimensional model of electrodeposition could possibly bring some hints for solving this important issue.

To explain both the stability of the envelope of the growth and the distance between the branches, comparison of the diffusion length and branch spacing is quite instructive. The set of experimental runs that we have already performed suggests that these two lengths are of the same order of magnitude for DBM. Nevertheless, the real situation is more com-

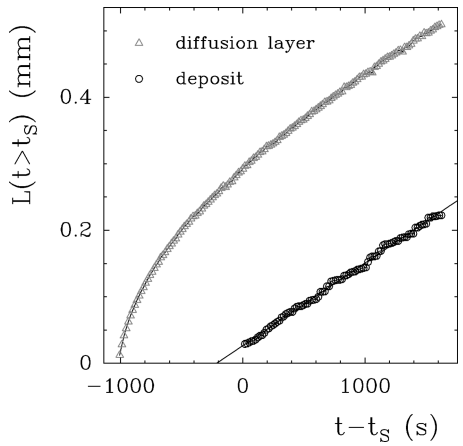

FIG. 11. Stationary dynamics in diffusoconvective growth experiments. The two curves show the propagation of both the diffusoconvective front and of the copper electrodeposit. $[Cu(SO_4)]=0.2$ mol l^{-1}, $j=8$ mA cm^{-2}, thickness of the cell 250 μm.

plex because the deposit cannot be characterized by a single length as we have done for the concentration field. As a matter of fact, the distance between the trees (d_t) and their width (w_t) are likely to be valuable parameters for modeling

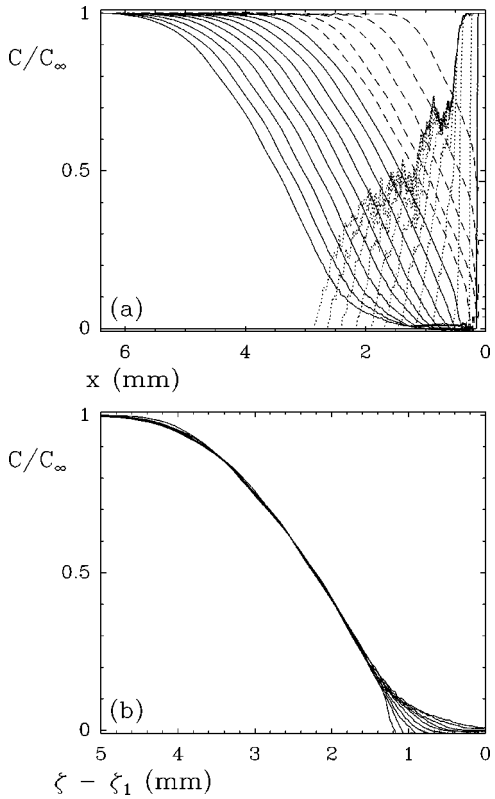

FIG. 12. (a) Concentration profiles measured by interferometry in diffusoconvective growth experiment, in dotted lines are represented the occupation ratio of the deposit in the cell, the concentration profiles prior to Sand's time are plotted in dashed. The time interval between each profile is ~167 s. (b) Superimposed concentration profiles obtained by a shift of the profiles of (a) (adjustment by hand) $[Cu(SO_4)]=0.2$ mol l^{-1}, $j=8$ mA cm^{-2}, thickness of the cell 250 μm.

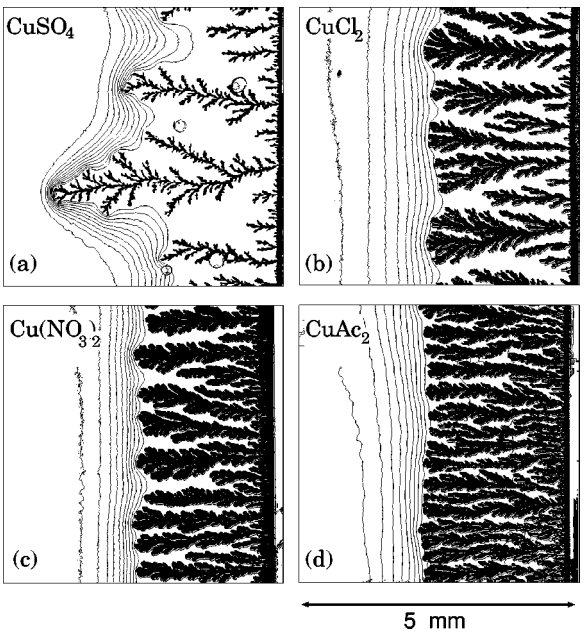

FIG. 13. Interferometric characterization of concentration maps around copper electrodeposits obtained from different copper salts. (a) Copper sulfate $[Cu(SO_4)]=0.5$ mol l^{-1}, $j=40$ mA cm^{-2}. (b) Copper chloride $[Cu(Cl_2)]=0.5$ mol l^{-1}, $j=27$ mA cm^{-2}. (c) Copper nitrate $[Cu(NO_3)_2]=0.5$ mol l^{-1}, $j=48$ mA cm^{-2}. (d) Copper acetate $[Cu(Ac)_2]=[Cu(CH_3COO)_2]=0.2$ mol l^{-1}, $j=12$ mAcm^{-2}.

the internal structure of the deposit. The copper concentration in a finger (related to its porosity) can probably be interpreted as arising from a microscopic instability [7,14] and is linked to the two macroscopic lengths of the deposit by the relation

$$\frac{C_\infty}{1-t^+}=C_{finger}\frac{w_t}{w_t+d_t}, \tag{18}$$

the latter ratio being the fraction of the cell that is filled by the deposit and $C_\infty/(1-t^+)$ the mean copper concentration in the deposit deduced from the expression for $\overline{\rho}$. The understanding of such a morphology selection lies beyond the scope of our one-dimensional analysis and deserves further experimental investigations.

IV. CONCLUSION

We have discussed here the occurrence of stationary growth dynamics in electrodeposition of copper. We have performed a quantitative analysis of these processes, based on interferometric measurements. We checked that these regimes can be described as 1D diffusion-limited processes and that the growth velocity varies as the inverse of the measured diffusion length, which describes the spreading of the depletion layer in front of the deposit. Although this picture happens to be quite relevant for describing the global dynamics, it describes neither the internal structure of the aggregates (in particular, the number of trees cannot be predicted by the 1D model) nor the stability of the flat growth enve-

lope. Moreover, the transition from the flat electrode to the stationary growth regimes cannot be described as a purely 1D process, since it involves a two-dimensional competition between the branches that emerge from the electrode after its instability. Finally, the generalization of these stationary growth regimes to thick cells where buoyancy driven convection is involved is discussed on an experimental example.

ACKNOWLEDGMENTS

We are very grateful to Y. Sorin and G. Gadret for their technical assistance with the optical setup. We thank A. Arneodo for stimulating and fruitful discussions. We are very grateful to the Center National d'Etudes Spatiales for supporting our work under Grant No. 97/CNES/071/6850.

[1] L. M. Sander, in *The Physics of Structure Formation*, edited by W. Guttinger and G. Dangelmayr (Springer-Verlag, Berlin, 1987), p. 257.
[2] T. Witten and L. Sander, Phys. Rev. Lett. **47**, 1400 (1981).
[3] T. Witten and L. Sander, Phys. Rev. B **27**, 5686 (1987).
[4] T. Vicsek, *Fractal Growth Phenomena* (World Scientific, Singapore, 1989).
[5] A. Kuhn, F. Argoul, J. Muzy, and A. Arneodo, Phys. Rev. Lett. **73**, 2998 (1994).
[6] F. Argoul, A. Arneodo, J. Elezgaray, and A. Kuhn, Fractals **5**, 75 (1997).
[7] J.-N. Chazalviel, Phys. Rev. A **42**, 7355 (1990).
[8] V. Fleury, J.-N. Chazalviel, M. Rosso, and B. Sapoval, J. Electroanal. Chem. **290,** 249 (1990).
[9] V. Fleury, M. Rosso, J.-N. Chazalviel, and B. Sapoval, Phys. Rev. A **44**, 6693 (1991).
[10] J. Melrose, Phys. Rev. Lett. **65**, 3009 (1990).
[11] J. Melrose, Chemom. Intell. Lab. Syst. **15**, 231 (1992).
[12] M. Bazant, Phys. Rev. E **52**, 1903 (1995).
[13] R. Aogaki, K. Kitazawa, Y. Kose, and K. Fueki, Electrochim. Acta **25**, 965 (1980).
[14] J. Elezgaray, C. Léger, and F. Argoul, J. Electrochem. Soc. **145**, 2016 (1998).
[15] D. Barkey and P. Laporte, J. Electrochem. Soc. **137**, 1655 (1990).
[16] C. Léger, J. Elezgaray, and F. Argoul, Phys. Rev. Lett. **78**, 5010 (1997).
[17] J. Huth, H. Swinney, W. McCormick, A. Kuhn, and F. Argoul, Phys. Rev. E **51**, 3444 (1995).
[18] A. Kuhn and F. Argoul, J. Electroanal. Chem. **397**, 93 (1995).
[19] J.-N. Chazalviel, M. Rosso, E. Chassaing, and V. Fleury, J. Electroanal. Chem. **407**, 61 (1996).
[20] J. Newman, *Electrochemical Systems* (Prentice-Hall, Englewood Cliffs, New Jersey, 1991).
[21] D. Otero, G. Marshall, and S. Tagtachian, Fractals **4**, 7 (1996).
[22] M.-Q. Lòpez-Salvans, P. Trigueros, S. Vallmitjana, J. Claret, and F. Sagues, Phys. Rev. Lett. **76**, 4062 (1996).
[23] M. Lopez-Salvans, F. Sagues, J. Claret, and J. Bassas, J. Electroanal. Chem. **421**, 205 (1997).
[24] J. B. F. Texier, L. Servant, and F. Argoul, J. Electroanal. Chem. **446**, 189 (1998).
[25] A. Bard and L. Faulkner, *Electrochemical Methods. Fundamentals and Applications* (Wiley, New York, 1980).
[26] Data Translation frame grabber (768×512) and public domain NIH Image program, developed at the U.S. National Institutes of Health and available on the Internet at http://rsb.info.nih.gov/nih-image/
[27] K. Crennell *et al.*, in *Interferogram Analysis*, edited by D. Robinson and G. Reid (Institute of physics publishing, Techno House, Redcliffe Way, Bristol, BS1 6NX, England, 1993).
[28] J. de Bruyn, Phys. Rev. E **56**, 3326 (1997).
[29] C. Léger and F. Argoul (unpublished).
[30] F. Argoul, E. Freysz, A. Kuhn, C. Léger, and L. Potin, Phys. Rev. E **53**, 1777 (1996).